# Optical Evaluation of Silicon Wafers With Rounded Rear Pyramids

Keith R. McIntosh, Ngwe Zin, Hieu T. Nguyen, Matthew Stocks, Evan Franklin, Kean C. Fong, Teng C. Kho, Teck K. Chong, Er-Chien Wang, Tom Ratcliff, Daniel Macdonald, and Andrew W. Blakers

***Abstract*—We investigate the light trapping in Si wafers that are textured with conventional random pyramids on their front surface and rounded random pyramids on their rear. It is well established that rounding the pyramids leads to better surface passivation, but whether or not it improves light trapping depends on the cell structure. In this paper, we apply ray tracing, spectrophotometry, and photoluminescence spectroscopy (PLS) to understand and quantify how rounding the rear pyramids might affect the light trapping in back-contact solar cells. We describe how rounding the pyramids leads to two competing optical effects: 1) reduced absorption in the rear films and 2) reduced scattering from the rear texture. The first effect improves light trapping whereas the latter degrades it. We show how the influence of each effect depends on wavelength and how they can be discerned (but not easily quantified) in reflectance curves. With PLS measurements, we conclude that for our sample structure and etch solution, the generation current is approximately constant for etch durations less than $\sim$60 s, and decreases significantly as the etch duration increases. Thus, by limiting the duration of the rounding etch, superior surface passivation can be attained without degrading the light trapping.**

***Index Terms*—Light trapping, photoluminescence spectroscopy (PLS), ray tracing, solar cells, texture.**

## I. Introduction

SURFACE texture enhances the light trapping in a solar cell by 1) redirecting rays so that they pass obliquely through the cell, and 2) increasing the internal reflectance so that rays pass more times across the cell. Texture morphologies that contain periodic patterns, such as brickwork, tiler's patterns, perpendicular slats, and tilted pyramids, tend to yield the best light trapping [1]–[4] but their implementation is limited by cost and practical implications. A widely used and commercially viable morphology is random upright pyramids [5]; it yields good light trapping, particularly when applied to both surfaces [1], [6]–[8].

A disadvantage of a pyramidal morphology is that it increases surface recombination [9]–[15]. Higher recombination occurs at a textured surface because it has a larger surface area and, depending on the passivating film, it can also have a higher density of interface states due to its <111>-oriented facets [12]–[15], epitaxial differences at the pyramid valleys [11], [16], microroughness [17], and possibly film stress [12]–[15], [18].

The surface recombination rate at random pyramids is decreased by chemically "rounding" the pyramids (e.g., in an HF:$HNO_3$ solution) [11], [12], [16], [19]–[28]. This rounding is also referred to as "polishing" or "planarizing" the pyramidal texture. Rounding the pyramids is rarely beneficial when applied to the front surface because the advantage of the lower recombination is outweighed by the disadvantage of higher external reflectance [12], [16], [19], [21], [22], but it has been found beneficial when applied to the rear surface of passivated-emitter rear-contact (PERC) solar cells [22], [23], [25], [26], [28]–[30]. Rounding the rear pyramids significantly improves the internal quantum efficiency (IQE) at long wavelengths, whether their rear passivation stack is $SiO_2$/$SiN_x$/Al [25], [28], $SiN_x$/Al [30], $Al_2O_3$/$SiN_x$/Al [25], [26], [30], $SiO_x$/$SiN_x$/Al [29], $Al_2O_3$/Al [22], or $SiO_2$/$SiO_x$/$SiN_x$/Al [23], correlating to an increase in short-circuit density of up to 2.0, 1.1, 0.6, 0.5, 0.5, and 0.4 mA/cm$^2$, respectively. This improvement is largely attributable to better rear surface passivation [22], [25], [26], [28], [30]. To a lesser extent, and as evident from reflectance measurements [22], [25]–[27], [29]–[31] and IQE measurements [23], rounding the rear pyramids also affects light trapping in PERC cells.

With varying degrees of thoroughness, the studies of [22], [28], [29], and [31] show that rounding the pyramids increases internal reflectance and decreases scattering—both of which increase the escape reflectance. Importantly, however, these two effects have opposing influences on the light trapping, and hence on the absorption in the Si wafer and $J_{\rm SC}$; that is, an increase in internal reflectance improves light trapping whereas a decrease in scattering degrades it. Consequently, whether rounded pyramids are superior to nonrounded pyramids—or even to a planar surface—depends on the degree of rounding and the properties of the rear films. (Even on a single sample set, differing analyses can yield differing conclusions as to whether rounding is beneficial or deleterious to light trapping [28].)

Manuscript received June 15, 2017; revised September 8, 2017; accepted September 12, 2017. This work was supported in part by Trina Solar and in part by the Australian Government through the Australian Renewable Energy Agency. *(Corresponding author: Keith R. McIntosh.)*

K. R. McIntosh is with PV Lighthouse, Coledale, NSW 2515, Australia (e-mail: krmcintosh@pvlighthouse.com.au).

N. Zin is with the Florida Solar Energy Center, University of Central Florida, Orlando, FL 32816 USA (e-mail: soe.zin@anu.edu.au).

H. T. Nguyen, M. Stocks, E. Franklin, K. C. Fong, T. C. Kho, T. K. Chong, T. Ratcliff, D. Macdonald, and A. W. Blakers are with the Research School of Engineering, Australian National University, Canberra, ACT 2601, Australia (e-mail: hieu.nguyen@anu.edu.au; matthew.stocks@anu.edu.au; evan.franklin@anu.edu.au; kean.fong@anu.edu.au; teng.kho@anu.edu.au; teck.chong@anu.edu.au; tom.ratcliff@anu.edu.au; daniel.macdonald@anu.edu.au; andrew.blakers@anu.edu.au).

E.-C. Wang is with the Solar Energy Research Institute of Singapore, National University of Singapore, 117574, Singapore (e-mail: er-chien.wang@anu.edu.au).

Color versions of one or more of the figures in this paper are available online at http://ieeexplore.ieee.org.

Digital Object Identifier 10.1109/JPHOTOV.2017.2754060

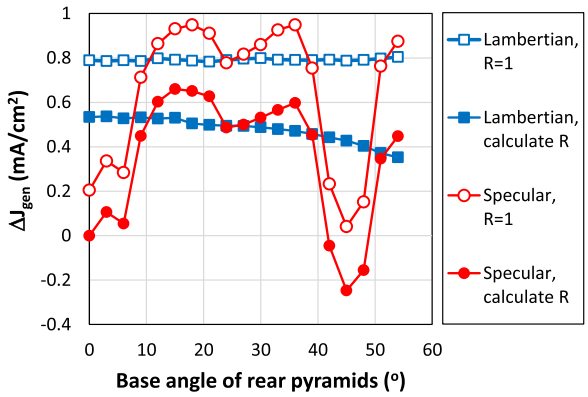


Fig. 1. Change in generation current $\Delta J_{\rm gen}$ relative to a planar rear surface, where the rear reflectance is either 100% (open symbols) or calculated by the transfer matrix method (solid symbols), and where the rear reflectance is either specular (red) or Lambertian (blue).

In this work, we use simulation, spectrophotometry, and photoluminescence spectroscopy (PLS) to further explore how rounding the rear pyramids affects light trapping. The selected films are relevant to high-efficiency solar cells such as an interdigitated back-contact (IBC) solar cell. A forerunner to this work was published in [32].

## II. Preliminary Evaluation by Ray Tracing

Fig. 1 presents a preliminary assessment on how modifying the rear pyramids influences light trapping. The figure plots the results of simulations conducted with the PV Lighthouse ray tracer [33] using the inputs listed in Appendix A. It shows how the base angle of the rear pyramids $\omega_{\rm rear}$ affects the generation current $\Delta J_{\rm gen}$ relative to the case of a planar rear surface ($\omega_{\rm rear} = 0°$), where a positive $\Delta J_{\rm gen}$ indicates an improvement in light trapping. The results are, of course, contingent on the cell geometry and materials; the inputs for this study represent a high-efficiency laboratory IBC solar cell [34], [35].

Fig. 1 plots four curves. Red and blue symbols show results for when the rear reflectance is specular and Lambertian. Open symbols show results for when the rear reflectance was 100%, and solid symbols show results for when it was calculated by the transfer matrix method (TMM).

The most relevant of the four curves is that with the solid red symbols. We expect this data to be the closest to a real sample since the reflectance from the rear facets is specular and calculated by TMM (i.e., it accounts for the rear films). Consistent with the simulations in [1] and [8], the results show that introducing conventional rear pyramids (e.g., $\omega_{\rm rear} \sim 53°$) improves light trapping and hence $\Delta J_{\rm gen}$. We also see that the highest $J_{\rm gen}$ is attained when $10° < \omega_{\rm rear} < 40°$, and that the poorest light trapping is attained when $\omega_{\rm rear} \sim 45°$ (even poorer than when the rear is planar $\omega_{\rm rear} = 0°$).

The observed dependence of $\Delta J_{\rm gen}$ on $\omega_{\rm rear}$ arises due to 1) differences in the fraction of second-pass rays that falls within the escape cone of the pyramid facets [1], and 2) an increase in absorption within the rear films as the incident angle increases. The first of these dependencies can be best evaluated by observing the curve with the open red symbols; this simulation neglected parasitic absorption in the rear films and it shows a minor dip at ~25° and a deeper dip at ~45°. The second of the dependencies is best evaluated by observing the curve with the solid blue symbols; this simulation removed the dependence on escape angles (because the Lambertian rear reflectance randomized the rays after the first pass) and it exhibits a monotonic decrease in $J_{\rm gen}$ with increasing $\omega_{\rm rear}$, amounting to 0.2 mA/cm$^2$ over the range 0–54°.

Fig. 1 also shows that relative to a planar and specular rear, Lambertian reflection increased $J_{\rm gen}$ by 0.55 mA/cm$^2$. This compares to ~0.8 mA/cm$^2$ calculated for one PERC structure [36]. Whether a truly Lambertian reflection can be formed without greatly increasing recombination is of interest but not the focus of this study. The figure indicates that with an appropriate angle, specular reflection can slightly exceed the Lambertian case, e.g., by 0.1 mA/cm$^2$ at 15°. Incidentally, simulating the same structure but with a second antireflection coating (ARC) as in [34], $\Delta J_{\rm gen}$ for the planar Lambertian case increases from 0.55 to 0.8 mA/cm$^2$; this relates to the double-layer ARC transmitting more light that falls within the critical angle of a front facet.

## III. Experimental Samples

The experiment contained seven samples. Their structure is summarized by Fig. 2 and Table I. Five of the samples (R0, R30, R60, R90, and R120) were included to represent IBC solar cells; they were textured with conventional random pyramids on their front surface and rounded random pyramids on their rear; their front was coated with a $SiN_x$ film and their rear with a $SiN_x$/Al thin-film stack. The remaining two samples had simpler structures and were included for comparison and to ensure the spectrophotometer was correctly calibrated; one was planar (sample P), the other was textured (sample T), and both were coated with a thin atomic-layer deposition (ALD) $AlO_x$.

The fabrication of the samples went as follows: high resistivity (>100 Ω/sq) n-type <100> silicon wafers were etched in tetramethylammonium hydroxide (TMAH) at 85 °C for 10 min to remove any saw damage. Random pyramids were formed on six of the seven wafers by following the conventional procedure of etching <100>-oriented Si wafers in an alkaline solution to expose <111>-oriented facets [37]. Specifically, the etch was performed at 85 °C for 60 min in a 4% TMAH solution that also contained isopropyl alcohol and Si seed crystals obtained from the precipitation of Si wafers in a 25% TMAH solution. Consequently, at this point of the process, both sides of six samples were textured with random pyramids and one sample remained planar. The effective base angle $\omega$ of the pyramids was found to be 53° (see Section IV-A).

After texturing, the front surface of the five "R samples" was coated with 7 $\mu$m of a polymer chemical mask to protect it from a room-temperature solution composed of 1:10 HF:$HNO_3$. This solution is well known to etch silicon isotropically, rounding the sharp peaks, ridges, and troughs of the pyramids, and thereby reducing their height and base angle. Table I lists the etch duration, the rear pyramid height, and the final thickness of each sample. By submitting the samples to differing etch durations, a

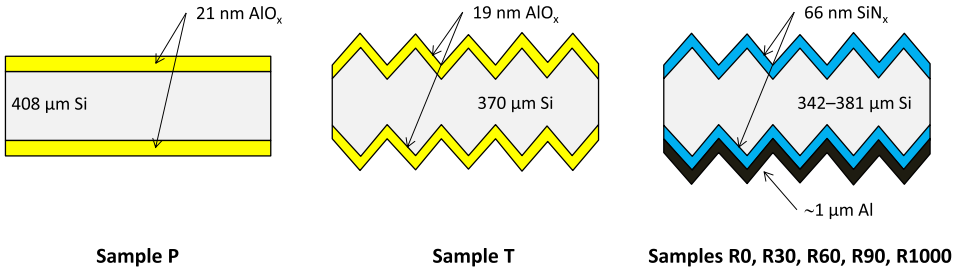


Fig. 2. Cross-sectional schematic of experimental samples.

TABLE I
EXPERIMENTAL SAMPLES

| Name | Thickness | Texture | | | | Thin-film coatings | |
|---|---|---|---|---|---|---|---|
| | ($\mu$m) | Front | Rear | Rear etch (s) | Rear height ($\mu$m) | Front | Rear |
| P | 408 | Planar | Planar | 0 | 0 | 21 nm $AlO_x$ | 21 nm $AlO_x$ |
| T | 370 | RP | RP | 0 | 6 | 19 nm $AlO_x$ | 19 nm $AlO_x$ |
| R0 | 381 | RP | RP | 0 | 6 | 66 nm $SiN_x$ | 66 nm $SiN_x$ and 1 $\mu$m Al |
| R30 | 375 | RP | RP | 30 | 3.5 | 66 nm $SiN_x$ | 66 nm $SiN_x$ and 1 $\mu$m Al |
| R60 | 371 | RP | RP | 60 | 2.5 | 66 nm $SiN_x$ | 66 nm $SiN_x$ and 1 $\mu$m Al |
| R90 | 364 | RP | RP | 90 | 1 | 66 nm $SiN_x$ | 66 nm $SiN_x$ and 1 $\mu$m Al |
| R120 | 339 | RP | RP | 120 | $< 1$ | 66 nm $SiN_x$ | 66 nm $SiN_x$ and 1 $\mu$m Al |

RP: random pyramids. "Rear height" is the maximum height of a rear pyramid detected within a 90 $\mu$m scan.

variety of rounded pyramids was attained. Confocal images of the surfaces were presented in [32].

Following the rounding etch, the polymer mask was removed from the "R samples" and ~66 nm of $SiN_x$ was deposited by plasma-enhanced chemical vapor deposition (PECVD) onto both sides. Next, about 1 $\mu$m of Al was evaporated onto their rear. The $SiN_x$ composition and thickness are typical of passivation layers and antireflection coatings, and the Al is typical of the rear contact and back reflector of the IBC solar cell. Approximately, 20 nm of $AlO_x$ was deposited by ALD onto the reference samples; the $AlO_x$ provided a good passivation layer for the reference samples because its dispersive refractive index is highly repeatable and, being so thin, it had little bearing on the optics. Both PECVD $SiN_x$ [14], [38] and ALD $AlO_x$ [39] provide very good surface passivation, contributing toward high a signal-to-noise in the PLS measurements.

The wafer thickness stated in Table I represents the average of four micrometer measurements at different locations on the wafer; the thickness of the front $AlO_x$ and $SiN_x$ was determined using the best-fit simulation of the front-surface reflection between 400 and 950 nm and the dispersive refractive index listed in Appendix A; the thickness of the rear $AlO_x$ and $SiN_x$ was assumed identical to the front films; and the thickness of the rear Al was estimated at 1 $\mu$m, where an accurate thickness for the Al is not required because it is much too thick to transmit photons within the wavelength range of interest.

## IV. SPECTROPHOTOMETRY

### A. External Reflectance ($300 < \lambda < 1000$ nm)

Fig. 3 plots the hemispherical reflectance from the front surface of all seven samples. The symbols show experimental data and the lines show best-fit simulations using OPAL 2 [40]. The best-fits were attained by varying the thickness of the front film and $\omega_{\text{front}}$ in the manner of [34].

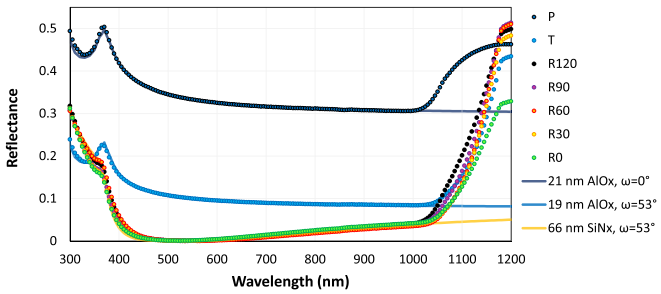


Fig. 3. Experimental reflectance (symbols) and simulated external reflectance (lines).

It is concluded that

1) the simulated data agree well with the experimental data;
2) $\omega_{\text{front}} = 53°$ gave the best fit, which is typical of our IBC texture process [34];
3) all of the rounded samples have a similar external reflectance ($\lambda < 1000$ nm), where best-fits were attained when the front $SiN_x$ thickness was $66 \pm 4$ nm; and
4) the escape reflectance differs between the rounded samples, indicative of differences in light trapping due to the rounded pyramids on the rear.

### B. Escape Reflectance ($1000 \leq \lambda \leq 1200$ nm)

Fig. 4 permits a better examination of the differences in light trapping between the samples. It plots the escape fraction $f_{\text{esc}}$ of 1) the samples with $SiN_x$/Al on their rear, and 2) the samples

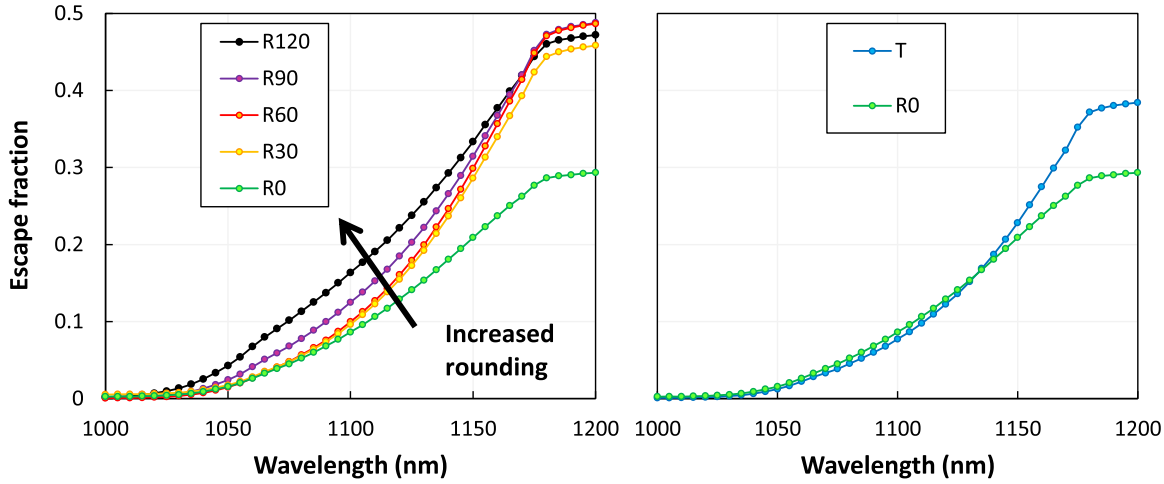


Fig. 4. Escape fraction of (a) samples with $SiN_x$/Al on the rear and (b) samples with no rounding.

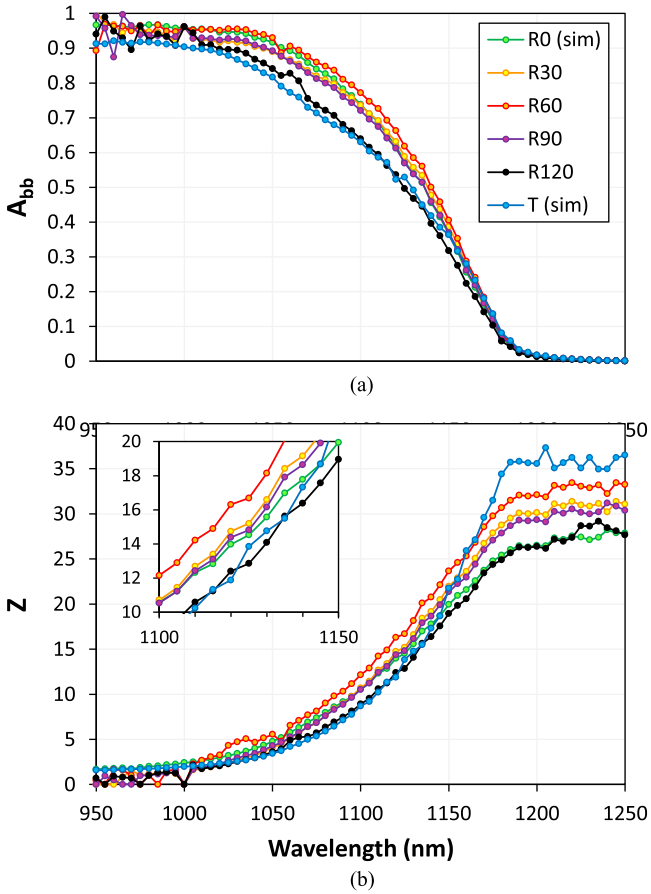


Fig. 5. (a) $A_{\mathrm{bb}}(\lambda)$ and (b) $Z(\lambda)$ of the textured samples, where the results for samples R0 and T are simulated, and the results for R30, R60, R90, and R120 are calibrated at all λ against R0; the inset in (b) shows a smaller range to highlight the differences between the curves at 1100–1150 nm.

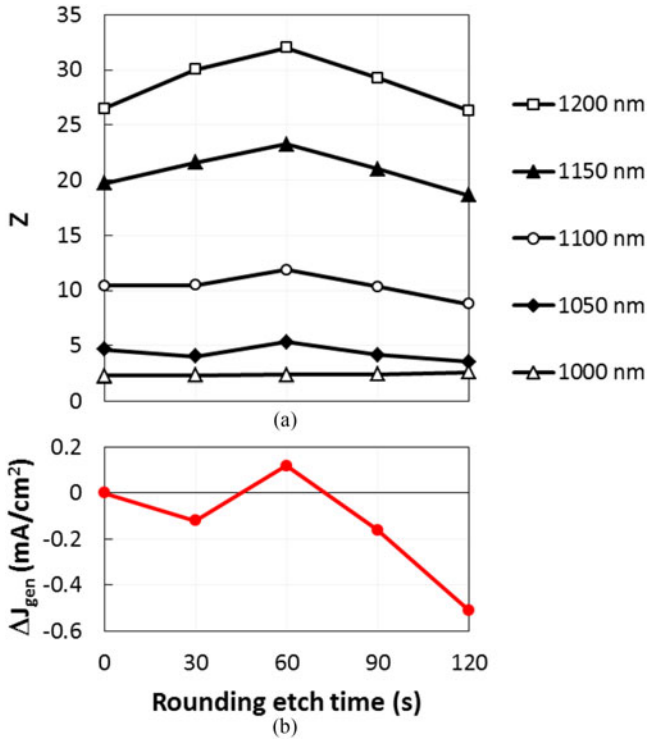


Fig. 6. (a) $Z(\lambda)$ at specific wavelengths and (b) $\Delta J_{\mathrm{gen}}(\lambda)$ over the range 1000–1250 nm for the AM1.5g spectrum.

with no rounding, where $f_{\mathrm{esc}}$ is the fraction of rays that having entered the silicon then escape through the front surface. It is defined by $f_{\mathrm{esc}} = R/(1 - R_{\mathrm{ext}})$, where $R_{\mathrm{ext}}$ is the external reflectance determined by the best-fit OPAL 2 simulation. The $x$-axis extends only over the range where $f_{\mathrm{esc}}$ is relevant for a Si solar cell ($1000 \leq \lambda \leq 1200$ nm).

It is evident from Fig. 4(a) that the rear rounding significantly alters the light trapping. Consistent with other studies on rounded rear pyramids [22], [23], [25]–[27], [29], [31], $f_{\mathrm{esc}}$ tends to be larger for samples with more rounding. We cannot, however, immediately conclude from the spectrophotometry results which sample has the best light trapping. A lower $f_{\mathrm{esc}}$ means there is more absorption in the sample, but does that absorption occur in the Si (better light trapping) or in the films (poorer light trapping)?

Since the samples are almost identical except for their rear morphology, differences in $f_{\rm esc}$ must arise predominantly from differences in the rear optics. There are two major competing effects:

First, sharper features mean that a downward traveling ray might bounce two or three times (and even four times for a small fraction of rays) from the facets of the rear pyramids before being propelled upwards. Each of those bounces reduces $f_{\rm esc}$ due to absorption in the $SiN_x$/Al films and, hence, they reduce the light trapping. The effect of this absorption on $f_{\rm esc}$ is compounded each time a ray returns to the rear surface. Consequently, rear absorption reduces $f_{\rm esc}$ more at long $\lambda$ where absorption in the silicon is weaker and hence rays interact more times with the rear surface.

Second, sharper features tend to introduce more scattering, which increases the average ray's traversal angle across the bulk of the wafer [1], thereby increasing its optical pathlength and the absorption in the Si. Thus, greater scattering at the rear should reduce $f_{\rm esc}$ and improve light trapping. For the samples of this study, differences in rear scattering will only be relevant to the first few optical passes because the front pyramids tend to randomize the light [41].

Thus, sharper rear features decrease $f_{\rm esc}$ either because of more absorption in the rear films, which affects $f_{\rm esc}$ more strongly at longer $\lambda$, or because of more scattering, which affects $f_{\rm esc}$ more strongly at shorter $\lambda$.

The trend in Fig. 4(a) at 1000–1150 nm indicates that $f_{\rm esc}$ is the highest for sample R120, then R90, and then R60, R30, and R0. This suggests that the degree of rear scattering did not change greatly until the duration of the rounding etch exceeded 60 s, at which point the scattering decreased, thereby reducing the light trapping.

The trend in Fig. 4(a) at $\lambda > 1150\,{\rm nm}$ indicates that $f_{\rm esc}$ is the highest for samples R120, R90, and R60, then R30, and then R0. Since R60, R30, and R0 exhibit a similar degree of rear scattering, this indicates that absorption in the rear $SiN_x$/Al decreases as the rounding etch increases. Notably, $f_{\rm esc}$ is considerably less for sample R0 at $\lambda = 1200\,{\rm nm}$, indicating that film absorption is much higher for the sample with no rounding.

The trends in Fig. 4(b) are also consistent with this discussion. At shorter $\lambda$, where scattering is more significant, we see that the nonrounded samples yield a similar $f_{\rm esc}$. At longer $\lambda$, where absorption in the rear $SiN_x$/Al must be more significant than in the $AlO_x$, $f_{\rm esc}$ is much lower for sample R0.

These and other spectrophotometry results [28], [29], [31] indicate that competing optical mechanisms arise when the rear pyramids are rounded. The rounding etch decreases scattering (reducing absorption in the Si) and decreases SiNx/Al absorption (leaving more light to be absorbed in the Si). We also conclude that the internal reflectance at the $SiN_x$/Al interface is poorer than having a thin $AlO_x$. The competing mechanisms prevent us from using spectrophotometry to discern the degree to which rounding alters the absorption in the Si, and hence the generation current. For that, we apply PLS.

Before describing the PLS results, we make a few remarks that were omitted above to avoid obfuscating the major conclusions:

1) The impact of free-carrier absorption could be neglected over the range 1000–1200 nm because the dopant concentration in the samples was very small ($<5 \times 10^{13}$ cm$^{-3}$) and the illumination intensity was very low.
2) Absorption in the front $SiN_x$ was negligible at long $\lambda$ and could be omitted from the analysis.
3) The reflectance at neither a Si/$SiN_x$ nor a Si/$SiN_x$/Al interface depends strongly on $\lambda$ over the range 1000–1200 nm.
4) In reference to the Lambertian case of Section II, scattering at the rear interface due to a small-scale structure would lead to less second-pass light intersecting the front pyramids within the escape cone of a facet.
5) To give an idea of why the escape reflectance changes so dramatically at long $\lambda$, the fraction of light absorbed during the light's first traversal across the wafer is 56% at 1050 nm, 16% at 1100 nm, 3% at 1150 nm, and 0.07% at 1200 nm (see Appendix B).

## V. Photoluminescence Spectroscopy

PLS [42]–[48] was employed to measure the samples' band-to-band absorption $A_{\rm bb}(\lambda)$ from which the optical pathlength enhancement $Z(\lambda)$ was calculated [48], [49]. These parameters quantify the degree of light trapping in the sample. The application of PLS to textured wafers is complicated by several sources of error that are otherwise insignificant for planar wafers, particularly when the illumination beam is focused as it is in our apparatus [48]. In such case, the apparatus must be calibrated at every wavelength by using a sample of known $A_{\rm bb}(\lambda)$ with similar optical properties to the measured samples. We used sample R0 for that purpose, where its $A_{\rm bb}(\lambda)$ was merely simulated by ray tracing (see Appendix A).

Figs. 5 and 6 present the results. Fig. 5 plots $A_{\rm bb}(\lambda)$ and $Z(\lambda)$, and Fig. 6 plots $Z$ at five specific wavelengths and $\Delta J_{\rm gen}$ for the AM1.5g spectrum, where zero represents the same $J_{\rm gen}$ as was simulated for R0. Both figures indicate that a short rounding etch improved light trapping slightly at all wavelengths but that longer etches degraded light trapping significantly.

It is helpful to understand the wavelength-dependence of the light trapping. Fig. 6(a) indicates that at 1200 nm, increasing the etch duration leads to a significant increase then a significant decrease in light trapping; this is consistent with experimental findings of PERC solar cells at 1200 nm [23]. Although advantageous, there is little absorption in the Si at 1200 nm, and hence the light trapping at shorter wavelengths has a stronger influence on the generation current.

We conclude from the PLS and spectrophotometry that a short rounding improves the rear reflectance without greatly reducing the rear scattering. This tends to yield an increase in $f_{\rm esc}(\lambda)$, $A_{\rm bb}(\lambda)$, and $Z(\lambda)$ at all $\lambda$ but is most observable in $f_{\rm esc}(\lambda)$ and $Z(\lambda)$ at long $\lambda$ (1150–1200 nm). As the rounding etch continues, however, it reduces the rear scattering while making little change to the rear reflectance. This tends to increase $f_{\rm esc}(\lambda)$ and decrease $A_{\rm bb}(\lambda)$ and $Z(\lambda)$ at all $\lambda$ but is most observable at shorter $\lambda$ (1000–1150 nm). For our structure and etch solution, the resulting light trapping is approximately constant for etch

durations less than ∼60 s, and then degrades for durations longer than 60 s.

We emphasize that the results from the PLS allow only a relative comparison between samples. The absolute values are uncertain because the calibration factor at each wavelength was determined such that the measured $A_{\rm bb}(\lambda)$ from sample R0 equaled its simulated $A_{\rm bb}(\lambda)$. Thus, the results for sample R0 are simply those from the simulation, and the results for the other samples are scaled equivalently. Systematic error might also have been introduced due to differences in the light trapping between samples. Thus, we can only be confident of the trends in Figs. 5 and 6, not the absolute values. Giving some credence to the absolute values, however, is that the experimental IQE of an IBC solar cell with similar films to these samples but a planar rear surface indicated that $Z \sim 25$ at $\lambda = 1200$ nm [34]; that cell structure is most similar to sample R120, for which we determined $Z = 27$ at 1200 nm.

Note that we did not use sample R0 as the calibration for the measurement of sample T because the optics of their front and rear surfaces are considerably different. The results for sample T in Fig. 5 are simply simulated and plotted for interest.

## VI. Conclusion

We examined the light trapping properties of textured silicon wafers whose rear pyramids were rounded and coated with $SiN_x$/Al. By considering the results of ray tracing, spectrophotometry, and PLS, we described the two competing effects that arise from rounding the rear pyramids:

1) The absorption in the $SiN_x$/Al decreases for short rounding times and then approximately saturates for longer rounding times. This arises because the incident rays bounce, on average, fewer times from the pyramid facets before being reflected upwards. Consequently, this leads to an increase in $f_{\rm esc}(\lambda)$, $A_{\rm bb}(\lambda)$ and $Z(\lambda)$ at all λ but more strongly at long λ (1150–1200 nm).
2) The degree of scattering from the rear surface decreases as the rounding time continues because the pyramids become flatter. Consequently, this leads to an increase in $f_{\rm esc}$ and decrease in $A_{\rm bb}$ and $Z(\lambda)$ at all λ but more strongly at shorter λ (1000–1150 nm).

For the sample structure and the etch solution we examined, these competing effects lead to $J_{\rm gen}$ being approximately constant for etch durations less than ∼60 s, and then decreasing as the etch duration increases above 60 s. This means that we can benefit from the improved surface passivation that arises from a short rounding etch with little change to the generation current.

## Appendix A: Ray Tracing Inputs

The ray tracing was performed with the PV Lighthouse online module ray tracer [33]. Table II lists the inputs that define the structure. In addition, the incident illumination was unpolarized and normally incident to the plane of the wafer; each simulation was comprised of 500 000 rays that were traced until the intensity of each ray was <0.01% of its starting intensity or until the ray had suffered >10 000 bounces; the incident wavelengths were swept from 900 to 1250 nm in 5 nm intervals, the generation current density was calculated with the AM1.5g spectrum; free-carrier absorption was neglected; and the polarization was accounted for at every interaction (i.e., it was not assumed that the TM:TE ratio was 1:1 at each interaction). These inputs led to a precision in $\Delta J_{\rm gen}$ of ±0.01 mA/cm$^2$. The dispersive refractive index (i.e., $n(\lambda)$ and $k(\lambda)$) of Si, $AlO_x$, $SiN_x$, $Si_3N_4$, and Al was taken from [50], [51], [52], [53] (for their sample with $n = 1.96$ at 632 nm), [34], and [54].

TABLE II
Inputs to the Ray Tracing Simulations

| Variable | IBC | Sample T | Sample R0 |
|---|---|---|---|
| *Random pyramid texture:* | | | |
| Texture width | 7 $\mu$m | 6 $\mu$m | 6 $\mu$m |
| Front base angle | 53° | 53° | 53° |
| Rear base angle | 0°, 3°, . . . , 51°, 54° | 53° | 53° |
| *Materials:* | | | |
| Front films | 73 nm $SiN_x$ | 19 nm $AlO_x$ | 66 nm $SiN_x$ |
| Substrate | 250 $\mu$m c-Si | 362 $\mu$m c-Si | 373 $\mu$m |
| Rear films | 30 nm $SiO_2$ | 19 nm $AlO_x$ | 66 nm $SiN_x$ |
| | 90 nm $Si_3N_4$ | | 1000 nm Al |
| | 1000 nm Al | | |

## Appendix B: First-Pass Absorptance

The approximate values for the first-pass absorptance $A_1$ were determined by assuming $A_1 = 1 - \exp(-\alpha W Z_1)$, where $\alpha$ is the absorption coefficient, $W$ is the wafer thickness, $Z_1 = 1/\cos(\theta_1)$, $\theta_1$ is the first-pass transmission angle and equal to $\varphi - a\sin[\sin(\varphi)/n]$, $n$ is the real refractive index, and $\varphi$ is the base angle of the pyramid. Hence, the calculation assumed that the only significant rays contributing toward $A_1$ are those that were transmitted directly into the silicon.

## References

[1] P. Campbell and M. A. Green, "Light trapping properties of pyramidally textured surfaces," *J. Appl. Phys.*, vol. 62, no. 1, pp. 243–249, 1987.
[2] P. Campbell, S. R. Wenham, and M. A. Green, "Light trapping and reflection control with tilted pyramids and grooves," in *Proc. 20th IEEE Photovolt. Spec. Conf.*, New York, NY, USA, 1988, pp. 713–716.
[3] P. Campbell, "Light trapping in textured solar cells," *Sol. Energy Mater.*, vol. 21, nos. 2–3, pp. 165–172, 1990.
[4] R. Brendel, "Simple prism pyramids: A new light trapping texture for silicon solar cells," in *Proc. 23rd IEEE Photovolt. Spec. Conf.*, New York, NY, USA, 1993, pp. 252–255.
[5] R. A. Arndt, J. F. Allison, and A. Meulenberg, "Optical properties of the Comsat non-reflective cell," in *Proc. 11th IEEE Photovolt. Spec. Conf.*, Scotttsdale, AZ, USA, 1975, pp. 40–43.
[6] D. Kray, M. Hermle, and S. W. Glunz, "Theory and experiments on the back side reflectance of silicon wafer solar cells," *Prog. Photovolt. Res. Appl.*, vol. 16, no. 1, pp. 1–15, 2008.
[7] J. Frank, M. Rüdiger, S. Fischer, J. C. Goldschmidt, and M. Hermle, "Optical simulation of bifacial solar cells," *Energy Procedia*, vol. 27, pp. 300–305, 2012.
[8] Z. C. Holman *et al.*, "Parasitic absorption in the rear reflector of a silicon solar cell: Simulation and measurement of the sub-bandgap reflectance for common dielectric/metal reflectors," *Sol. Energy Mater. Sol. Cells*, vol. 120, pp. 426–430, 2014.
[9] R. R. King, R. A. Sinton, and R. M. Swanson, "Studies of diffused phosphorus emitters - Saturation current, surface recombination velocity, and quantum efficiency," *IEEE Trans. Electron Devices*, vol. 37, no. 2, pp. 365–371, Feb. 1990.

[10] S. W. Glunz *et al.*, "Emitter dark saturation currents of high-efficiency solar cells with inverted pyramids," in *Proc. 13th Eur. Photovolt. Sol. Energy Conf.*, Nice, France, 1995, pp. 409–412.
[11] L. Fesquet *et al.*, "Modification of textured silicon wafer surface morphology for fabrication of heterojunction solar cell with open circuit voltage over 700 mV," in *Proc. 2009 34th IEEE Photovolt. Spec. Conf.*, 2009, pp. 000754–000758.
[12] K. R. McIntosh and L. P. Johnson, "Recombination at textured silicon surfaces passivated with silicon dioxide," *J. Appl. Phys.*, vol. 105, 2009, Art. no. 124520.
[13] S. C. Baker-Finch and K. R. McIntosh, "The contribution of planes, vertices and edges to recombination at pyramidally textured surfaces," *IEEE J. Photovolt.*, vol. 1, no. 1, pp. 59–65, Jul. 2011.
[14] Y. Wan and K. R. McIntosh, "On the surface passivation of textured c-Si by PECVD silicon nitride," *IEEE J. Photovolt.*, vol. 3, no. 4, pp. 1229–1235, Oct. 2013.
[15] L. E. Black, T. C. Kho, K. R. McIntosh, and A. Cuevas, "The influence of orientation and morphology on the passivation of crystalline silicon surfaces by Al2O3," *Energy Procedia*, vol. 55, pp. 750–756, 2014.
[16] M. G. Kang, S. Tark, J. C. Lee, C.-S. Son, and D. Kim, "Changes in efficiency of a solar cell according to various surface-etching shapes of silicon substrate," *J. Cryst. Growth*, vol. 326, no. 1, pp. 14–18, 2011.
[17] H. Angermann *et al.*, "Optimisation of electronic interface properties of a-Si: H/c-Si hetero-junction solar cells by wet-chemical surface pretreatment," *Thin Solid Films*, vol. 516, no. 20, pp. 6775–6781, 2008.
[18] P. J. Cousins and J. E. Cotter, "Minimizing lifetime degradation associated with thermal oxidation of upright randomly textured silicon surfaces," *Sol. Energy Mater. Sol. Cells*, vol. 90, no. 2, pp. 228–240, 2006.
[19] M. J. Cudzinovic and K. R. McIntosh, "Process simplifications to the Pegasus solar cell—SunPower's high-efficiency bifacial silicon solar cell," in *Proc. 29th IEEE Photovolt. Spec. Conf.*, New Orleans, LA, USA, 2002, pp. 70–73.
[20] H. Jin, K. J. Weber, and A. W. Blakers, "Depassivation of Si-$SiO_2$ interface following rapid thermal annealing," in *Proc. 4th World Conf. Photovolt. Energy Convers.*, 2006, pp. 1078–1080.
[21] M. Edwards, S. Bowden, U. Das, and M. Burrows, "Effect of texturing and surface preparation on lifetime and cell performance in heterojunction silicon solar cells," *Sol. Energy Mater. Sol. Cells*, vol. 92, no. 11, pp. 1373–1377, 2008.
[22] A. Dastgheib-Shirazi, M. Steyer, J. Junge, S. Gindner, and G. Hahn, "A study of the surface morphology of silicon: Effect of parasitic emitter etching on the rear side performance of silicon solar cells," in *Proc. 25th Eur. Photovolt. Sol. Energy Conf. Exhib. 5th World Conf. Photovolt. Energy Convers.*, 2010, pp. 2107–2113.
[23] E. Cornagliotti *et al.*, "How much rear side polishing is required? A study on the impact of rear side polishing in PERC solar cells," in *Proc. 27th Eur. Photovolt. Sol. Energy Conf. Exhib.*, 2012, pp. 561–566.
[24] G. Li, Y. Zhou, and F. Liu, "Influence of textured c-Si surface morphology on the interfacial properties of heterojunction silicon solar cells," *J. Non-Cryst. Solids*, vol. 358, no. 17, pp. 2223–2226, 2012.
[25] C. Kranz *et al.*, "Impact of the rear surface roughness on industrial-type PERC solar cells," in *Proc. 27th Eur. Photovolt. Sol. Energy Conf.*, Frankfurt, Germany, 2012, pp. 557–560.
[26] C. Kranz *et al.*, "Wet chemical polishing for industrial type PERC solar cells," *Energy Procedia*, vol. 38, pp. 243–249, 2013.
[27] R. Maxi, P. Saint-Cast, T. Dannenberg, M. Zimmer, and J. Rentsch, "Impact of rear side roughness on optical and electrical properties of a high-efficiency solar cell," *Energy Procedia*, vol. 77, pp. 832–839, 2015.
[28] C. Schwab *et al.*, "Recombination and optical properties of wet chemically polished thermal oxide passivated Si surfaces," *IEEE J. Photovolt.*, vol. 3, no. 2, pp. 613–620, Apr. 2013.
[29] J. Horzel *et al.*, "Development of rear side polishing adapted to advanced solar cell concepts," in *Proc. 26th Eur. Photovolt. Sol. Energy Conf.*, 2011, pp. 2210–2216.
[30] A. Cacciato *et al.*, "Investigating manufacturing options for industrial PERL-type Si solar cells," *Sol. Energy Mater. Sol. Cells*, vol. 113, pp. 153–159, 2013.
[31] N. Wöhrle, J. Greulich, C. Schwab, M. Glatthaar, and S. Rein, "A predictive optical simulation model for the rear-surface roughness of passivated silicon solar cells," *IEEE J. Photovolt.*, vol. 3, no. 1, pp. 175–182, Jan. 2013.
[32] N. Zin *et al.*, "Rounded rear pyramidal texture for high efficiency silicon solar cells," in *Proc. 2016 IEEE 43rd Photovolt. Spec. Conf.*, 2016, pp. 2548–2553.
[33] [Online]. Available: www.pvlighthouse.com.au. Accessed on: May 26, 2017.
[34] K. R. McIntosh *et al.*, "Quantifying the optical losses in back-contact solar cells," in *Proc. 40th IEEE Photovolt. Spec. Conf.*, Denver, CO, USA, 2014, pp. 115–123.
[35] E. Franklin *et al.*, "Design, fabrication and characterisation of a 24.4% efficient interdigitated back contact solar cell," *Prog. Photovolt.*, vol. 24, pp. 411–427, 2014.
[36] T. Lauermann, B. Fröhlich, G. Hahn, and B. Terheiden, "Design considerations for industrial rear passivated solar cells," in *Proc. 2012 38th IEEE Photovolt. Spec. Conf.*, 2012, pp. 001710–001715.
[37] L. M. Landsberger, S. Naseh, M. Kabrizi, and M. Paranjape, "On hillocks generated during anisotropic etching of Si in TMAH," *J. Microelectromech. Syst.*, vol. 5, pp. 106–116, 1996.
[38] M. J. Kerr, J. Schmidt, A. Cuevas, and J. H. Bultman, "Surface recombination velocity of phosphorus-diffused silicon solar cell emitters passivated with plasma enhanced chemical vapor deposited silicon nitride and thermal silicon oxide," *J. Appl. Phys.*, vol. 89, pp. 3821–3826, 2001.
[39] B. Hoex, J. Schmidt, P. Pohl, M. C. M. Van de Sanden, and W. M. M. Kessels, "Silicon surface passivation by atomic layer deposited $Al_2O_3$," *J. Appl. Phys.*, vol. 104, no. 4, 2008, Art. no. 044903.
[40] K. R. McIntosh and S. C. Baker-Finch, "OPAL 2: Rapid optical simulation of silicon solar cells," in *Proc. 38th IEEE Photovolt. Spec. Conf.*, Austin, TX, USA, 2012, pp. 265–271.
[41] R. Brendel, "Couple of light into mechanically textured silicon solar cells: A ray tracing study," *Prog. Photovolt.*, vol. 3, pp. 25–38, 1995.
[42] T. Trupke, E. Daub, and P. Wurfel, "Absorptivity of silicon solar cells obtained from luminescence," *Sol. Energy Mater. Sol. Cells*, vol. 53, pp. 103–114, 2003.
[43] T. Trupke, J. Zhao, A. Wang, R. Corkish, and M. A. Green, "Very efficient light emission from bulk crystalline silicon," *Appl. Phys. Lett.*, vol. 82, pp. 2996–2998, 2003.
[44] C. Schinke, D. Hinken, J. Schmidt, K. Bothe, and R. Brendel, "Modeling the spectral luminescence emission of silicon solar cells and wafers," *IEEE J. Photovolt.*, vol. 3, no. 3, pp. 1038–1052, Jul. 2013.
[45] C. Barugkin, N. S. Zin, and K. R. Catchpole, "Photoluminescence enhancement towards high efficiency plasmonic solar cells," in *Proc. 39th IEEE Photovolt. Spec. Conf.*, Tampa, FL, USA, 2013, pp. 0025–0028.
[46] C. Barugkin, Y. Wan, D. Macdonald, and K. R. Catchpole, "Evaluating plasmonic light trapping with photoluminescence," *IEEE J. Photovolt.*, vol. 4, no. 4, pp. 1292–1297, Oct. 2013.
[47] C. Barugkin *et al.*, "Light trapping efficiency comparison of Si solar cell textures using spectral photoluminescence," *Opt. Express*, vol. 23, pp. A391–A400, 2015.
[48] K. R. McIntosh *et al.*, "Experimental errors that arise when applying photoluminescence spectroscopy to textured silicon wafers," submitted for publication.
[49] J. A. Rand and P. A. Basore, "Light-trapping silicon solar cells experimental results and analysis," in *Proc. 22nd IEEE Photovolt. Spec. Conf.*, Las Vegas, NV, USA, 1991, pp. 192–197.
[50] M. A. Green, "Self-consistent optical parameters of intrinsic silicon at 300K including temperature coefficients," *Sol. Energy Mater. Sol. Cells*, vol. 92, no. 11, pp. 1305–1310, 2008.
[51] H. T. Nguyen, F. E. Rougieux, B. Mitchell, and D. H. Macdonald, "Temperature dependence of the band-band absorption coefficient in crystalline silicon from photoluminescence," *J. Appl. Phys.*, vol. 115, 2014, Art. no. 043710.
[52] P. Kumar, M. Wiedmann, C. Winter, and I. Avrutsky, "Optical properties of Al2O3 thin films grown by atomic layer deposition," *Appl. Opt.*, vol. 48, no. 28, pp. 5407–5412, 2009.
[53] S. Duttagupta, F. Ma, B. Hoex, T. Mueller, and A. Aberle, "Optimised antireflection coatings using silicon nitride on textured silicon surfaces based on measurements and multidimensional modeling," *Energy Procedia*, vol. 15, pp. 78–83, 2012.
[54] E. Palik, *Handbook of Optical Constants of Solids Vol I*, Orlando, FL, USA: Academic Press, pp. 397–400, 1985.

Authors' photographs and biographies not available at the time of publication.